ADVANCED OPTICAL MATERIALS

www.advopticalmat.de

Light-Stimulated Charge Transport in Bilayer Molecular Junctions for Photodetection

*Shailendra K. Saxena, Scott R. Smith, Mustafa Supur, and Richard L. McCreery**

Eleven bilayer molecular junctions (MJs) consisting of two different 5–7 nm thick molecular layers between conducting contacts are investigated to determine how orbital energies and optical absorbance spectra of the oligomers affect the photocurrent (PC) response, the direction of photoinduced charge transport, and maximum response wavelength. Photometric sensitivity of 2 mA W^{-1} and a detection limit of 11 pW are demonstrated for MJs, yielding an internal quantum efficiency of 0.14 electrons per absorbed photon. For unbiased MJs, the PC tracks the absorption spectrum of the molecular layer, and is stable for >5 h of illumination. The organic/organic (O/O) interface between the molecular layers within bilayer MJs is the primary determinant of PC polarity, and the bilayer MJ mechanism is conceptually similar to that of a single O/O heterojunction studied in bilayers of much greater thickness. The charge transport direction of the 11 MJs is completely consistent with hole-dominated transport of photogenerated carriers. For MJs illuminated while an external bias is applied, the PC greatly exceeds the dark current by factors of 10^2 to 10^5, depending on bias, bilayer structure, and wavelength. The bilayer MJs are amenable to flexible substrates, and may have applications as sensitive, wavelength-specific photodetectors.

1. Introduction

Stimulation of charge transport by incident light has long been studied and exploited in both inorganic and organic semiconductors, with familiar examples being the charge-coupled device, photodiodes, photocells, and light-emitting diodes. For organic semiconductors such as thin-film transistors and organic photovoltaic devices, transport distances generally exceed 50 nm since spin coating is a common fabrication technique. When the charge transport distances in organic electronic devices are below ≈15 nm, the realm of molecular electronics emerges, with often very different transport mechanisms such as coherent tunneling[1] and field ionization.[2] Molecular junctions (MJs) consisting of single molecules or arrays of parallel molecules between conducting contacts have been studied extensively.[1,3] The field is driven in part by the possibility of new electronic functions in molecular devices and the wide variety of molecular structures available, presumably with a broad range of electronic behaviors.[4] "Large area" or "ensemble" MJs with partially transparent contacts enable the use of optical spectroscopy for characterization and monitoring of molecular electronic devices using infrared absorption,[5] Raman,[6] and UV-vis spectroscopy.[4d,7]

While optical spectroscopy is normally a probe of device structure during fabrication and operation, the field of "molecular optoelectronics" investigates stimulation of transport with light or generation of light in response to an external bias.[8] Photocurrent (PC) generation and changes in MJ conductance by incident light have been reported for single molecules and molecular ensembles and examined theoretically.[4a,9] We have reported PCs and photoconductance changes in carbon-based MJs, mediated by internal photoemission (IPE)[10] and optical absorption in the molecular layer.[11] The observed PC tracks the in situ UV-vis absorption spectrum of the molecular layer when the transport distance exceeds 5 nm, and the PC polarity (i.e., the charge transport direction) and induced photovoltage correlate strongly with which orbitals mediate transport (highest occupied molecular orbital (HOMO) or lowest unoccupied molecular orbital (LUMO)).[11b] Carbon-based MJs also exhibit photoemission from hot electrons,[8c,12] and transport in thiol-based large-area MJs can couple to plasmons in the contacts to emit light.[8d,13]

For PCs in unbiased, Au/carbon/molecule/carbon/Au MJs with identical top and bottom electrodes, the direction of illumination did not cause a change in PC sign, indicating that there must be some inherent asymmetry in the device. We attributed the asymmetry in single-component carbon-based MJs to a difference in electronic coupling at the two electrode contacts, one of which is covalent and the other physisorbed.[11b] This effect was predicted theoretically by Galperin et al.[8b,14] Since the internal electric field generated by the effect is small (10–30 mV), the resulting PCs are also small for single-component MJs, and would likely be absent if the electronic coupling to both electrodes were identical. We recently reported a different approach in which a molecular bilayer was used to create asymmetry, leading to significantly larger PCs.[15] Successive reduction of two diazonium reagents[16] resulted in a covalent

Dr. S. K. Saxena, Dr. S. R. Smith, Dr. M. Supur, Prof. R. L. McCreery
Department of Chemistry
University of Alberta
11227 Saskatchewan Dr., Edmonton, Alberta T6G 2G2, Canada
E-mail: richard.mccreery@ualberta.ca

The ORCID identification number(s) for the author(s) of this article can be found under https://doi.org/10.1002/adom.201901053.

DOI: 10.1002/adom.201901053

Table 1. Summary of single-layer PC and molecular orbitals energies.

Oligomer subunit		DFT[a)] HOMO [eV]	TD-DFT LUMO [eV]	DFT |H-L| [eV]	Abs λ_{max} [eV]	PC λ_{max} [eV]	Peak PC yield [e^- per photon]
Anthraquinone[b)]	AQ	−7.00	−2.79	4.21	4.80	4.13	-3.2×10^{-5}
Nitroazobenzene	NAB	−6.65	−3.04	3.61	3.54	3.54	-7.2×10^{-5}
Fluorene	FL	−5.74	−0.71	5.03	4.69	4.28	$+2.8 \times 10^{-5}$
Bis-thienyl benzene	BTB	−5.29	−1.48	3.81	3.46	3.44	$+4.0 \times 10^{-4}$
Tetraphenyl porphyrin	TPP	−4.92	−2.19	2.73	2.88	2.88	$+1.79 \times 10^{-4}$

[a)]Molecular orbital energies were calculated using DFT on Gaussian 09 at B3LYP 6–31g(d) level of theory; [b)]Molecular structures are provided in Scheme S1 in the Supporting Information.

bilayer of oligomers of anthraquinone (AQ, 5–7 nm thick) and bis-thienyl benzene (BTB, 7–8 nm). The PC and photovoltage of the bilayer MJ were much larger than for either single layer, and the sign of the PC was reversed when the order of deposition of the two layers was also reversed. In addition, the bilayer PC spectrum peaked at the optical absorption maximum of BTB, and exhibited a shoulder peak near the absorption maximum of AQ. Unlike many existing photosensitive and photovoltaic devices,[17] the carbon-based bilayer MJs used electron beam–deposited carbon (eC) for both electrodes, and did not rely on a work function difference to drive observed PCs.

The current investigation was undertaken to determine the generality of bilayer PCs in MJs and to determine how the photoresponse of covalent bilayer MJs varies with molecular structure and orbital energies. The role of electronic coupling at both electrodes and at the organic/organic (O/O) interface between the molecular layers as well as the effect of an applied bias are considered, and the results provide useful conclusions about the mechanism of PC generation. These insights should prove valuable in designing photosensitive devices with particular optical and electronic properties, possibly leading to sensitive molecular photodetectors with narrow wavelength selectivity which are amenable to a variety of substrate materials.

2. Results

Device fabrication and PC measurements were conducted as described previously,[11a,15] and all structures had identical electrodes using eC, denoted as Au_{30}/eC_{10}/molecular layer/eC_{10}/Au_{20}. The subscripts indicate layer thicknesses in nm and the molecular layers consisted of one or two of the components listed in **Table 1**. Device structure is shown schematically in **Figure 1**A, along with the sign convention used to indicate negative PC, i.e., electron flow from the bottom to top electrode in the external circuit. Conversely, positive PC corresponds to

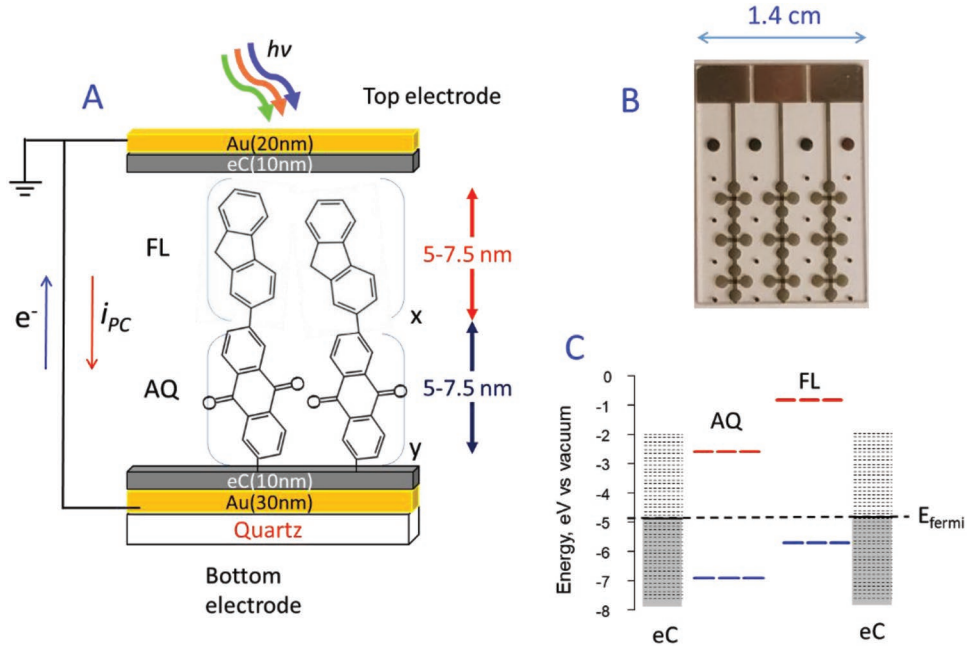

Figure 1. A) Schematic of a $Au_{30}/eC_{10}/AQ_6/FL_6/eC_{10}/Au_{20}$ bilayer MJ structure containing AQ and FL oligomeric layers. eC is electron beam–deposited carbon. Light enters through an ≈30% transparent top contact as shown, and bias values are stated as the bottom electrode relative to the top. B) Optical image of a completed quartz chip containing nine MJs. C) Energy levels for frontier orbitals of AQ and FL relative to vacuum, with red indicating LUMO and blue indicating HOMO. Horizontal dashed line indicates the Fermi level of the e-beam carbon.

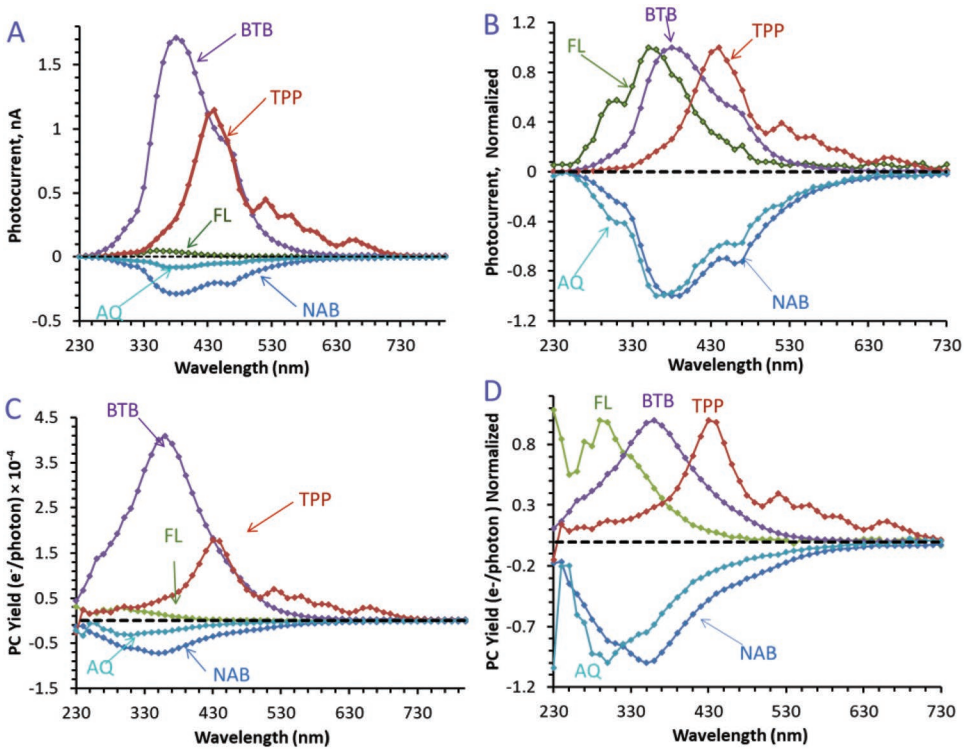

Figure 2. A) Uncorrected PC spectra for five single-layer MJs containing 5–7 nm layers of AQ, NAB, FL, BTB, and TPP. B) Normalized PC spectra from panel (A). C) PC yields in electrons/incident photon determined from source output power in Figure S3E of Supporting Information. D) Normalized PC yields from panel (C).

electron flow from the top to bottom electrodes in the external circuit. Additional fabrication details including molecular layer thicknesses are provided in Sections S1 and S2 in the Supporting Information, and Figure 1B is an optical image of a completed sample with nine MJs. Table 1 includes calculated orbital energies for isolated single molecules and the maximum UV-vis absorption energy predicted by time-dependent density functional theory (TD-DFT) calculations. The energy levels for an AQ/fluorene (AQ/FL) bilayer junction are shown in Figure 1C, referenced to the vacuum level.

Although free molecule orbital energies are often significantly perturbed from interactions with the electrodes in the solid state, they do provide an initial approximation for designing devices. The optical absorption energies for single-component layers were determined in completed large-area devices, as the difference between the absorbance of a "blank" $Au_{30}/eC_{10}/eC_{10}/Au_{20}$ electrode and a completed single-layer MJ, as described previously.[4d,11b] Table 1 shows that the absorption maxima predicted from TD-DFT are approximately equal to the experimentally observed in situ absorbance maxima in intact MJs. The in situ UV-vis absorption spectra for single-component MJs are provided in Figure S2 in the Supporting Information. **Figure 2**A shows the PC spectra for single-layer MJs which are uncorrected for variations in incident light intensity with wavelength, and Figure 2B displays the same spectra after normalization of the maximum response to ±1.0. PC magnitudes should be considered approximate, since they depend on molecular layer thickness, number of incident photons, and electrode transmission, but the PC sign is reliable and provides useful information about energy level alignment.[11b] After measurement of the source intensity spectrum, the PC was converted to PC yield as electrons per incident photon[11b] or external quantum efficiency (EQE), as described in Section S4 in the Supporting Information. Figure 2C shows PC yield versus wavelength for single-component MJs, and the corresponding peak PC magnitudes and photon energies are listed in Table 1. The qualitative similarity of the tetraphenylporphyrin (TPP) absorption and the PC yield spectra confirms the previous observation that PC tracks the optical absorption of the molecular layer for BTB, AQ, and nitroazobenzene (NAB).[11b] Normalized spectra of Figure 2B,D highlight the clear differences in spectrum shape and maximum response for the five single-layer MJ structures.

Bilayer MJs consisting of 11 different combinations of single components were constructed by successive reduction of the appropriate diazonium reagents.[16,18] In all cases, the thicknesses (d) determined by atomic force microscopy "scratching" were 5–7.5 nm for each layer, with the deposition conditions and measured thicknesses listed in Table S1 in the Supporting Information. Bilayers are designated with the first layer on the left and the second on the right, e.g., AQ/FL refers to the structure illustrated in Figure 1A, and the second listed component is always closest to the illumination source in the current experiments unless noted otherwise. **Figure 3**A shows PC yield spectra for four bilayers having AQ as the first component and the single-layer spectrum for AQ alone. The AQ/BTB example was presented previously,[15] but repeated here to assure identical fabrication conditions across the bilayers studied. The

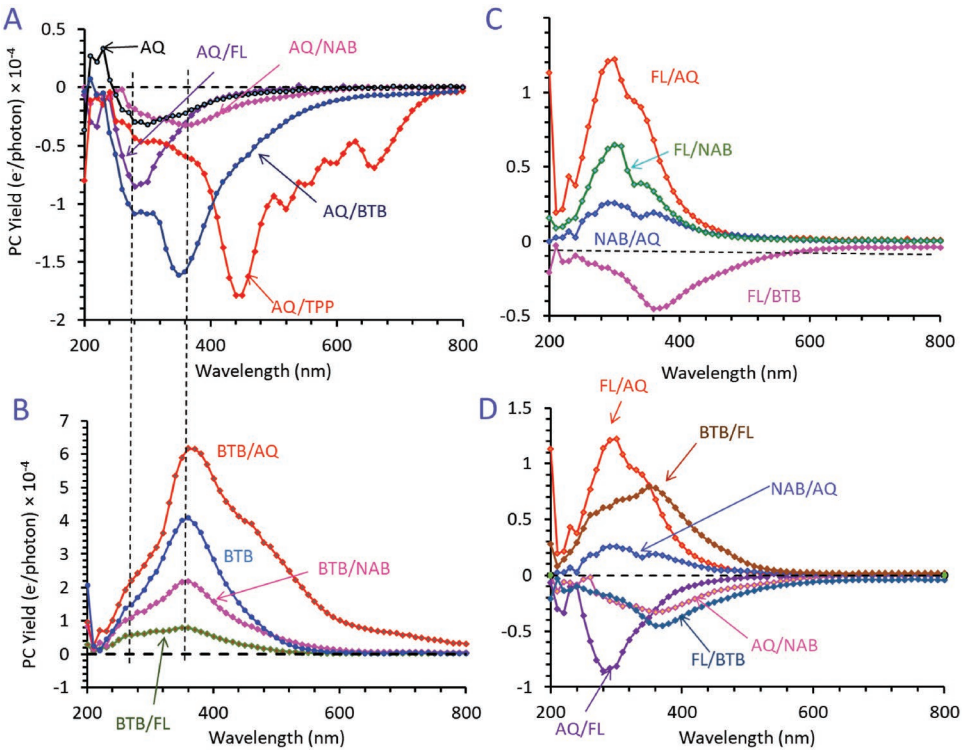

Figure 3. PC yields for 11 bilayer MJs with molecular layer thicknesses of 5–7.5 nm. A) PC yield for four bilayer MJs having AQ as a first (bottom) layer and single-layer AQ. B) PC yield for four bilayers MJs having BTB as a first (bottom) layer and single-layer BTB as a reference. C) Additional bilayers not shown in panel (A) or (B). D) PC yield spectra for three pairs of bilayer MJs with the layer order reversed. Vertical dashed lines in panels (A) and (B) indicate the absorption maxima of AQ (264 nm) and BTB (356 nm).

dark current/voltage response was unchanged by 407 nm laser illumination (Figure S7B, Supporting Information), and as discussed below, AQ is an electron acceptor with a low-lying LUMO energy (–2.79 V vs vacuum) and the uniformly negative observed PCs indicate electron flow away from the AQ electrode in the external circuit (as shown in the AQ/FL example in Figure 1A). Figure 3B compares three bilayers with BTB as the first component, and Figure 3C presents the additional four bilayer combinations to reach a total of 11 bilayer MJs studied. Note that the PC sign, magnitude, and spectrum shape vary significantly for the various combinations, even though the thicknesses of all individual molecular layers are in the range of 5–7.5 nm (Table S1, Supporting Information). The vertical dashed lines in Figure 3A,B indicate that the MJs containing BTB all have a PC feature close to the absorption maximum of BTB (356 nm) and the AQ containing MJs have a peak or shoulder at AQ's absorption maximum (264 nm). Figure 3D shows PC yield spectra for three bilayer pairs in which the layer order was reversed: FL/AQ, FL/BTB, and NAB/AQ. As noted previously for AQ/BTB,[15] reversal of the layer order caused reversal of PC sign accompanied by approximate reversal of the PC magnitude. The result is reversal of the relative magnitudes of the HOMO and LUMO energy levels of the two layers, which controls transport direction as discussed below. However, reversal of the direction of illumination from top to bottom as shown in Figure S6 in the Supporting Information did not change the PC sign for any of the MJs studied. Bilayers with NAB as the first layer were difficult to make reliably, likely due to irreversible reduction of the nitro group during the second layer deposition, similar to that reported by in situ Raman spectroscopy of MJs.[6f] **Table 2** summarizes the wavelengths, energies, signs, and magnitudes of the 11 bilayer examples shown in Figure 3.

The in situ UV-vis absorption spectra of the bilayer devices were determined in the same manner as single layers[4d,11b] to assess optical absorption in the presence of electronic coupling or other effects which might alter absorption compared to free molecules in solution. Figure S4 in the Supporting Information shows the example of the AQ/TPP bilayer spectrum before and after subtraction of absorption by the substrate and electrodes. **Figure 4** compares several in situ absorption spectra to the PC yield spectra for bilayers, and additional comparisons are provided in Figure S5 in the Supporting Information. Not surprisingly, the bilayer absorption spectra are dominated by the stronger absorber, although the UV region below 280 nm was difficult to acquire due to the relatively small absorbance of the molecular layers compared to that of the electrodes. For BTB/FL, BTB/NAB, and AQ/TPP, the bilayer PC yield spectra correlate closely with UV-vis absorption, as was the case for single-layer MJs.[11b] Note that photon absorption in the eC or Au contacts can also occur, and may result in IPE observed previously for very thin layers (d = 2–4 nm) of oxides[19] and molecules[10] in partially transparent devices. IPE in single-layer devices is very weak when d exceeds 4 nm,[11] hence the PC spectrum is weakly dependent on light absorption by the contacts. For AQ/FL in Figure 4D, the absorption and PC peaks

Table 2. Bilayer UV-vis absorption maxima and PCs.

Molecule	λ^{PC}_{max} for photocurrent [nm]	Max PC energy [eV]	Max absorption energy [eV]	Peak PC yield [e⁻ per photon]
AQ/FL	300	4.13	4.67	-8.1×10^{-5}
AQ/NAB	350	3.54	3.49	-3.2×10^{-5}
AQ/TPP	451	2.75	2.81	-1.8×10^{-4}
AQ/BTB	360	3.44	3.44	-1.6×10^{-4}
NAB/AQ	280	4.42	4.59	$+2.6 \times 10^{-5}$
FL/AQ	289	4.28	4.80	$+1.2 \times 10^{-4}$
FL/NAB	300	4.13	3.69	$+6.4 \times 10^{-5}$
FL/BTB	360	3.44	3.52	-4.5×10^{-5}
BTB/NAB	360	3.44	3.47	$+2.4 \times 10^{-4}$
BTB/AQ	360	3.44	3.44	$+6.1 \times 10^{-4}$
BTB/FL	370	3.35	3.49	$+7.8 \times 10^{-5}$

do not precisely match, but that may be partly due to the short wavelengths and the difficulty of subtracting the "blank" device spectrum. The close correspondence of the six absorption features of AQ/TPP with PC yield clearly indicates the importance of molecular absorption for PC generation. Table 2 includes cases which contain oligomers with the same two structures but different order (AQ/FL, AQ/BTB, BTB/FL). For eight of the 11 combinations, the maximum PC energy is within 0.1 eV of the maximum UV-vis absorption energy, and the remaining three are in the less accurate UV region below 300 nm.

We noted previously that increasing the thickness of the AQ layer in BTB/AQ bilayers decreased the observed PC yield, by ≈85% when the AQ layer was increased from 5.4 to 16 nm.[15] This thickness dependence was examined here for two additional examples, AQ/FL and FL/NAB, shown in **Figure 5**. For all nine bilayer combinations, the PC magnitude and PC yield decreased when either molecular layer increased in thickness, with the highest PC always observed for the thinnest molecular layers. For FL/NAB in Figure 5C, the PC decreases even when the stronger absorber (NAB) increases in thickness from 5 to 9.5 nm. Combined with the previously reported BTB/AQ results, the results imply that the O/O interface is important for PC generation, and dominates the PC response even when more light is absorbed in thicker layers. If PC generation and charge separation occur only at or near the O/O interface, then thicker molecular layers would result in transport losses or

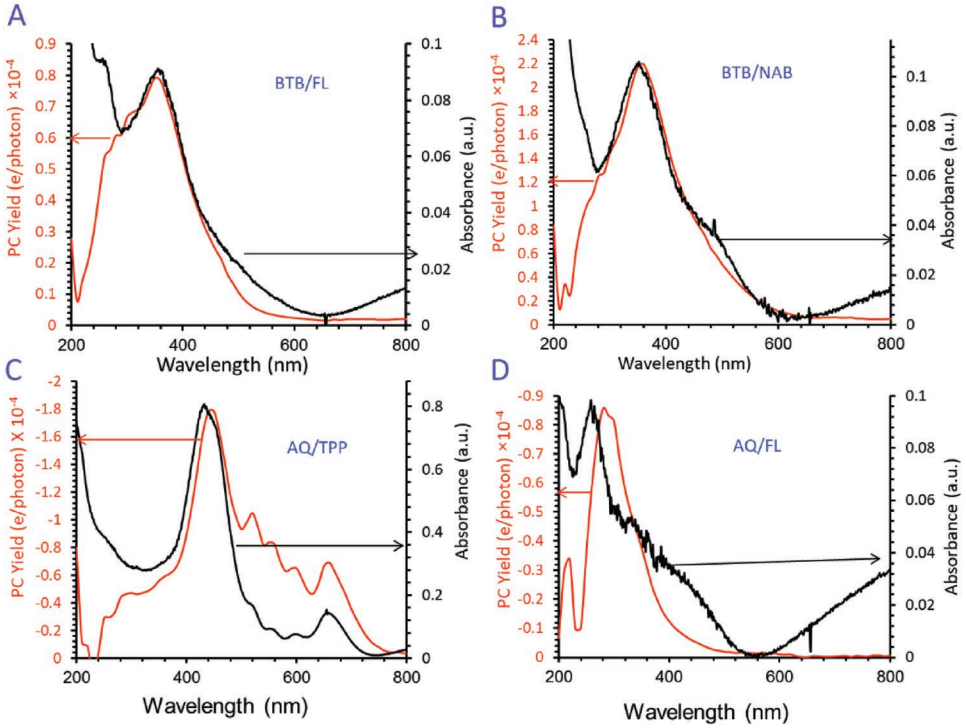

Figure 4. A) Overlays of PC and PC yield spectra and absorption spectra for A) BTB/FL, B) BTB/NAB, C) AQ/TPP, and D) AQ/FL. The PC yield in panel (A) ranged from 0 to 0.9×10^{-4} e⁻ per photon. Absorption spectrum of Au/C/C/Au electrode was subtracted from each molecular spectrum.

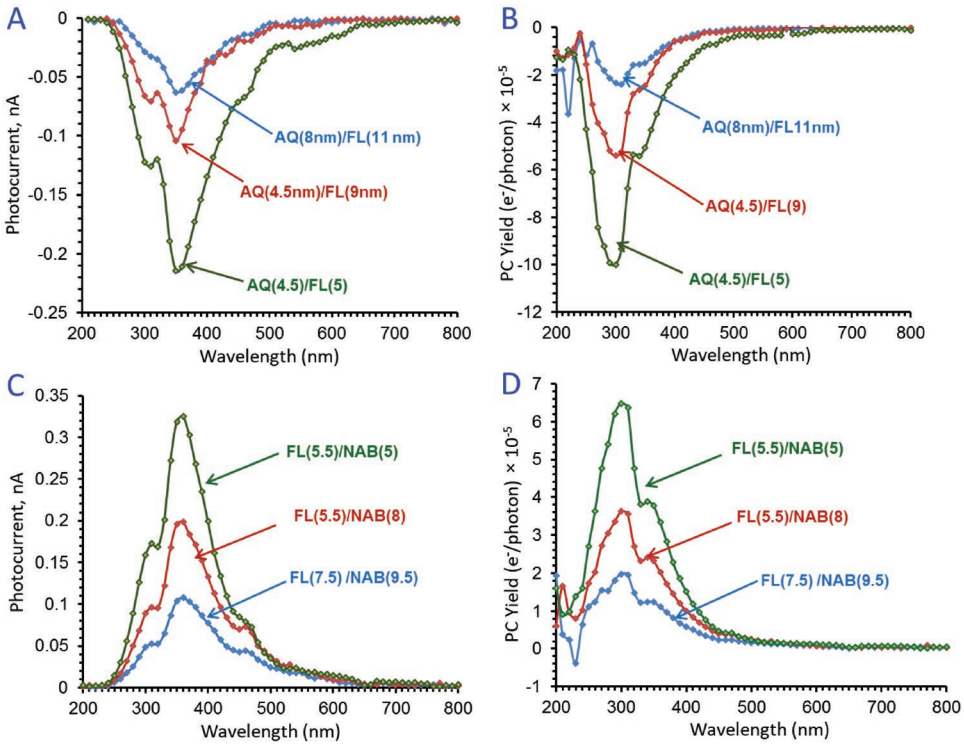

Figure 5. Overlays of A,C) PC and B,D) PC yields spectra of indicated bilayer MJs showing the effect of molecular layer thickness. Layer thicknesses (nm) are indicated for each spectrum in parentheses.

recombination which would decrease carriers reaching the electrodes and external circuit.

The results thus far involved unbiased MJs, but we reported recently that *JV* curves of single-component layers obtained under illumination can reveal distinct mechanistic differences between the dark and PC responses.[11a] An example is shown in **Figure 6**A for a BTB single-layer MJ ($d = 12.8$ nm) in the dark and illuminated with increasing power from a 407 nm diode laser. The increase in current under illumination is a factor of 2.0–4.5 for the range of $V = 0.2$–0.9 V for laser power of 0.30 W cm^{-2}. The PC increases linearly with light intensity and has a *JV* shape similar to the dark current. The BTB/AQ bilayer response shown in Figure 6B exhibits an offset for PC = 0 from near zero (<5 mV) for BTB alone to +0.37 V for BTB/AQ, and a much larger increase in PC compared to the dark current of a factor of 91 at $V = 0.2$ V and 6400 at $V = -0.5$ V. The PC magnitude is lower for BTB/AQ than BTB with similar thickness (see **Table 3**), due in part to the much larger currents observed for BTB compared to AQ in the dark (a factor of $>10^4$ @ 0.5 V and $d = 10$ nm).[20] While the PCs are smaller for BTB/AQ, the "gain" of PC over dark current exceeds 10^5 @ $V = -0.67$ V, as indicated in Table 3. As shown in Figure 6C, the PC increases linearly with laser power for several bias values, but with widely differing slopes and variations in PC polarity. The photoeffect was completely reversible, with the dark response recovered after illumination was halted (Figure S7B, Supporting Information), and a slow decline in magnitude of <5% over 5.8 h (Figure S7C, Supporting Information). Figure 6D shows the response for the reversed AQ/BTB device, with a similarly large photoeffect and a polarity change in the open circuit voltage (OPV) to −0.11 V. Table 3 lists dark and PCs for the three cases shown in Figure 6 at bias values of ±0.5 and ±1.0 V, and the bias voltage where the maximum PC gain (i.e., light over dark current) was observed. Figure S9 in the Supporting Information shows the ratio of light to dark current for the three MJs on a log scale, with the ratio varying by five orders of magnitude in the ±1 V bias range. While the magnitude of the PC gain depends strongly on thickness and bias voltage, the maximum observed for BTB alone (12.8 nm) was 150 at $V = -0.005$ V, 2300 for NAB (7.5 nm) at 0.1 V,[11a] 5.2×10^5 for BTB/AQ at −0.67 V, and 4.4×10^4 for AQ/BTB at −0.52 V. Obviously the bilayer PC responses under bias are much stronger than those for single layers, with significant changes in shape, polarity, and OPV compared to the dark responses. Using the definition of detection limit (LOD) as the incident light intensity which produces three times the standard deviation of the dark current, the LOD for BTB/AQ at $V = -0.67$ V is 10.8 pW on a junction area of 0.00125 cm^2.

3. Discussion

The results extend the previously reported observations for PCs in AQ/BTB bilayers to the nine additional bilayers listed in Table 2, which include a wider range of molecular properties, notably the HOMO and LUMO energies listed in Table 1. By keeping the electrode composition and layer thicknesses equal across the series of 11 bilayer structures, the effects of energy levels on PC spectrum and polarity were assessed. Several aspects previously observed for AQ/BTB[15] were retained

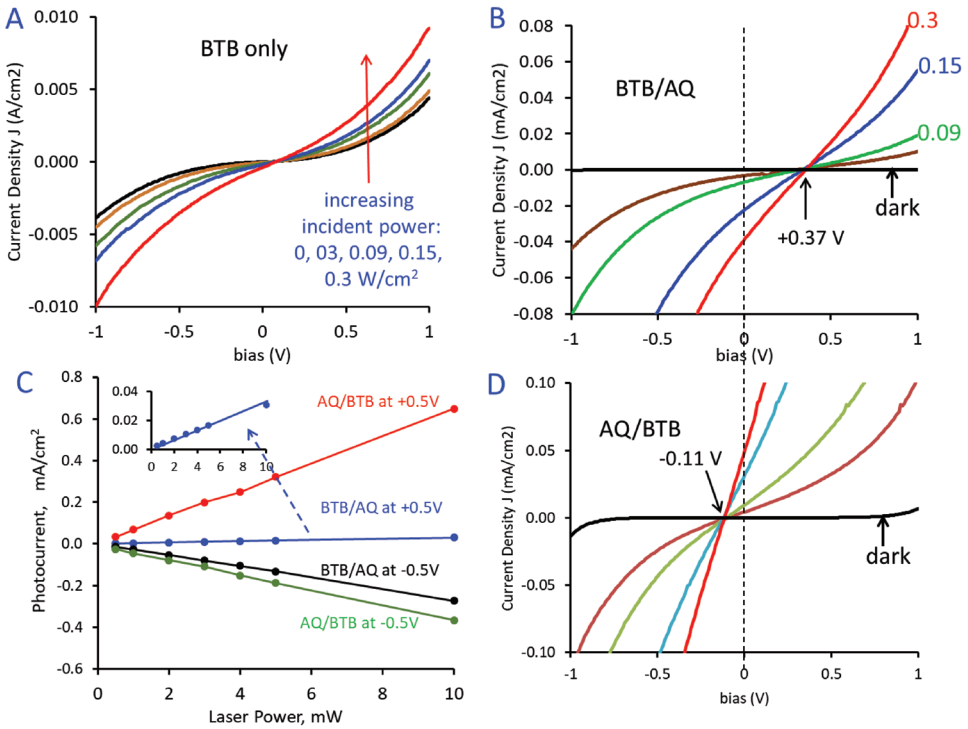

Figure 6. Current density under 407 nm laser illumination for various power densities ranging from 0 to 0.30 W cm^{-2} for A) BTB single layer (12.5 nm), B) BTB/AQ bilayer, and D) AQ/BTB bilayer MJs. C) PC density as a function of laser power for indicated bilayers and bias values. Vertical dashed line across panels (B) and (D) at $V = 0$ illustrates the polarity change in the OPV with the order of the molecular layers.

across the entire bilayer series, including independence of the direction of illumination (through top or bottom contacts) and reversal of the polarity when the layer order is reversed. As observed for single-layer MJs, the PC spectra shown in Figure 2 are strongly dependent on molecular structure, and track the absorbance of the molecular layer inside the completed MJ (Figure 4). In the case of TPP, the four additional absorption features (Q-bands) in the 500–700 nm range are reproduced

Table 3. PCs under bias for BTB, AQ/BTB, and BTB/AQ.

Molecule, bias	Dark current [nA]	PC, 407 nm, 0.30 W cm^{-2} [nA]	PC/dark ratio0.30 W cm^{-2}
AQ/BTB			
$V = 0.5$ V	0.206	812	3.94×10^3
1.0 V	8.49	1940	2.29×10^2
–0.5 V	0.017	–457	-2.65×10^4
–1.0 V	–17.1	–1530	8.92×10^1
–0.52 V	–0.011	–486	(Max) 4.42×10^4
BTB/AQ			
0.5 V	0.080	38.1	4.75×10^2
1.0 V	0.165	243	1.47×10^3
–0.5 V	0.028	–342	-1.24×10^4
–1.0 V	–0.413	–917	2.22×10^3
–0.67 V	0.0009	–464	(Max) -5.15×10^5
BTB only			
0.5 V	1107	3437	3.10
1.0 V	5518	11 500	2.08
–0.5 V	–1004	–4476	4.46
–1.0 V	–4830	–12 400	2.57
0.005 V	971	–429	(Max) –441

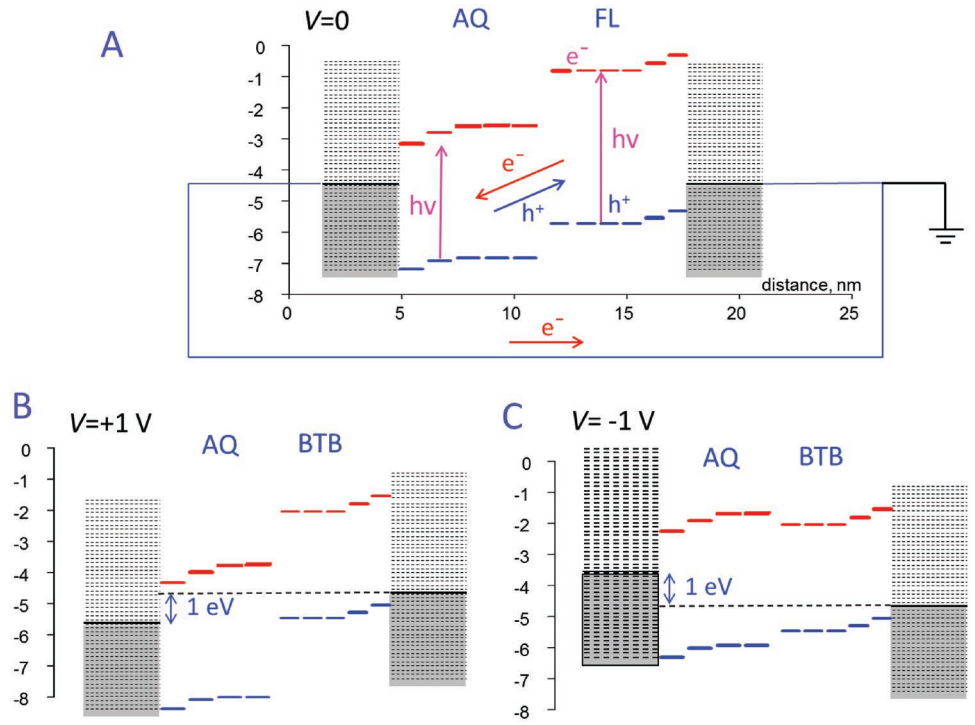

Figure 7. A) Schematic of a possible mechanism for PC production in an AQ/FL bilayer MJ at zero bias, with HOMO orbitals blue and LUMOs red. B) Same junction with the AQ electrode biased at +1 V relative to the FL layer. C) Same device with −1 V bias applied.

in the PC spectrum, confirming that photon absorption in the molecular layer rather than the contacts is the primary process underlying PC generation.

For the single-layer devices with d >5 nm, the sign of the PC for eight different molecular structures correlates with which frontier orbital, HOMO or LUMO, is closest to the electrode Fermi level, E_F.[11b] As shown in Figure 2, the "acceptor" molecules with low-lying LUMOs (AQ and NAB) yield negative PC in single-layer MJs, corresponding to electrons exiting the bottom electrode into the external circuit, while "donors" such as FL, BTB, and TPP have HOMOs close to E_F and exhibit positive PCs. The PC sign of single-layer MJs at zero bias is determined by asymmetric coupling between the bottom (i.e., covalent) and top electrodes which produces an internal electric field which drives the PC.[8b,11b,14] In bilayers, not only will coupling to the electrodes differ considerably since different molecules are involved, but there is also an O/O interface between the molecular layers with its own charge transfer and possible local shifts in electrostatic potential. The free molecule energy levels for AQ and FL shown in Figure 1B will be modified by electronic coupling with the electrodes, with one possible result for the completed bilayer shown in **Figure 7**A. In this case, FL would be considered a donor molecule which generates an upward potential shift of both HOMO and LUMO energies at the right (top) electrode, while AQ is an acceptor with a potential shift of the opposite polarity (but not necessarily equal in magnitude to that from FL). The magnitudes of the local potential shifts at the electrodes and the O/O interface are difficult to assess, although their existence and consequences have been discussed in significant detail, in the context of Fermi level pinning, vacuum level shifts, and interface dipoles.[21] For Figures 2–5, the combination of electrode/molecule and O/O interfaces results in an internal electric field which drives the PC, with electrons moving to the left in the molecular layer of Figure 7A. The magnitudes and direction of the internal electric field and potential shifts at the electrodes and O/O interface will vary with the molecular structure and the electronic coupling to the electrodes, but in the AQ/FL case shown electrons flow from the bottom (AQ) electrode to the top (FL), and the PC is negative. The generation of carriers may occur by photon absorption in either one of the bilayer molecules, but is dominated by the stronger absorber, yielding the strong similarity of absorption and PC spectra shown in Figure 4. As noted previously, the zero-bias PC spectrum can have features related to both molecular components,[15] but its polarity depends on the relative magnitudes of the interfacial potential shifts. At least at zero bias, the potential shifts determine the PC polarity, rather than which bilayer molecule absorbs the photon. Furthermore, the internal electric field at zero bias is determined by the molecules and electrodes, so the direction of illumination does not change the PC polarity.

A principle motive for studying bilayer PCs was determination of how molecular orbital energy levels affect PC polarity and magnitude, as a component of the "molecular signature" relating the structure to electronic behavior. While the donor/acceptor (D/A) model common in organic photodiodes and photocells[11a,17,22] agrees with the polarities of the PC observed for D/A examples in the current MJs, several cases involve two "donor" molecules (FL/BTB) or two "acceptors" (AQ/NAB), resulting in uncertainty about using the D/A model. The current results provide a consistent correlation relating orbital energies to PC polarity, illustrated in **Figure 8**. The DFT energy

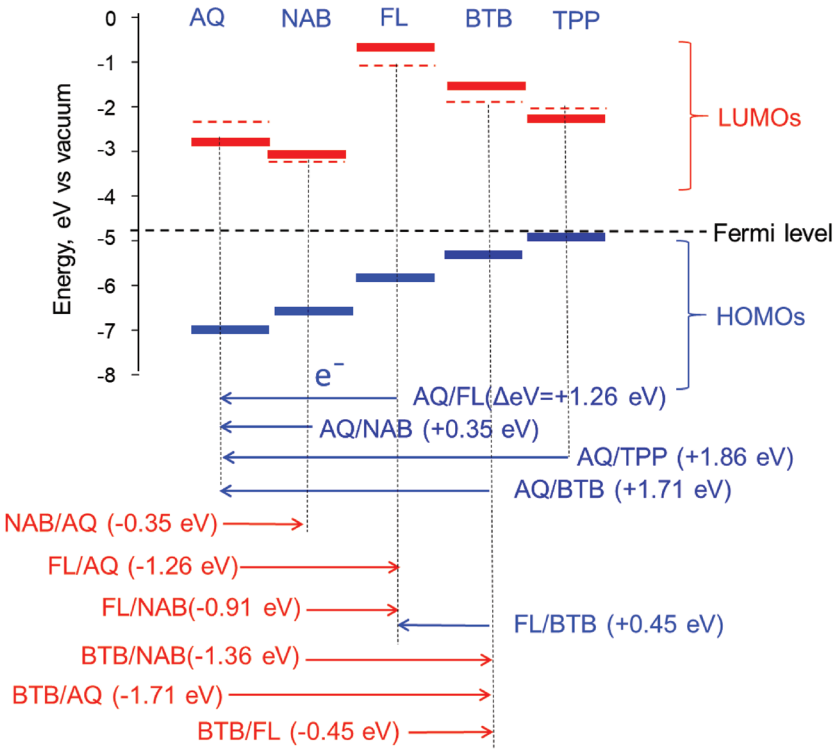

Figure 8. Correlation of the PC polarity and molecular orbital energies with the molecules arranged from left to right by increasing HOMO energy. Heavy lines are orbital energies from DFT (Table 1) and nearby dashed lines are determined from the DFT HOMO level and the in situ optical absorption maximum. Fermi level of eC (dashed black line) by UV photoelectron spectroscopy is −4.83 V versus vacuum.[4d] Red arrows indicate positive observed PC and blue arrows show negative PC yield. The length of arrows shows the difference of HOMOs energies for particular bilayer combination which qualitatively corresponds to PC magnitude. ΔeV is the DFT-predicted change in HOMO level in parentheses after the bilayer label.

levels from Table 1 are shown, arranged arbitrarily from left to right in order of the free molecule HOMO levels. As already noted, these levels are perturbed by electronic coupling and level shifts, but they at least provide a starting point for comparison. Below the energy levels are all 11 bilayer PC observations, listed in the same order as Table 2. The arrows indicate the direction of electron flow within the bilayer for each case, with blue indicating negative PC in the external circuit and red indicating positive. Since the molecules are arranged in order of HOMO energies, the longer arrows correspond to larger differences between the two HOMOs of the bilayer, and the difference in HOMO energies is indicated in Figure 8 as "ΔeV" after each bilayer label. Starting with the AQ/XX bilayer series shown in Figure 3B, all four examples yield negative PC, and all four second layers have HOMO energies higher than AQ. No such correlation is observed for the molecular LUMOs determined from TD-DFT, nor with the LUMO energies based on the observed in situ absorbance maximum (dashed lines in Figure 8). For the remaining seven bilayer examples, the PC polarity always corresponds to electron motion from the molecule with higher HOMO energy to that with lower, and no apparent correlation exists with the LUMO energies. In addition, the largest PCs occur for the largest difference in HOMO energy (AQ/BTB, 1.7 eV) and AQ/TPP (1.9 eV), and the smallest PC for the closest HOMO energies (NAB/AQ, 0.35 eV) and FL/BTB (0.45 eV). It is possible to attribute the HOMO correlation to activated electron transfer from the higher HOMO energy into a hole created in the lower energy HOMO by photon absorption, and such a mechanism should be distinguishable from the temperature dependence of bilayer PCs.

The open circuit photovoltages of single-layer MJs under illumination were <50 mV for FL[11b] and NAB,[11a] indicating that the internal potential drops from differential electronic coupling to the electrodes is typically <50 mV. The bias range of ±1 V used for Figure 6 is much larger, implying that the applied bias should overcome the internal potential shifts at the electrode and O/O interfaces. The AQ/BTB example is shown schematically in Figure 7B for a bias of +1 V. The applied voltage adds to the internal field and further increases the orbital energy difference at the O/O interface, thus increasing the device current as observed in Figure 6D. As the bias is scanned negatively, the internal electric field eventually exceeds that at zero bias and changes direction, resulting in the PC sign change for $V < -0.11$ V. The energy diagrams of Figure 7 are approximate and qualitative, and the actual OPVs and internal electric fields depend on several factors in addition to unperturbed energy levels. The slopes of the lines in Figure 6C are direct indications of photometric sensitivity, which varies with both wavelength and bias. For AQ/BTB and $V = +0.5$ V, the slope is 2.1 mA W^{-1} @407 nm, corresponding to an EQE of 0.64%, which increases to 2.8% at $V = +1$ V. The photometric "gain" equal to the illuminated current divided by the dark current at a given bias and wavelength increases from 2 to 5 for single-layer BTB to $>5 \times 10^5$ for the BTB/AQ bilayer biased at −0.67 V (Table 3). The magnitude of the gain for different bias values is determined by the current–voltage behaviors of both the dark and illuminated currents, which have different mechanisms and vary differently with bias, as is apparent in Figure S9 in the Supporting Information. The highest gains listed in Table 3 occur when the dark current is minimized, and further improvements should be possible through changes in molecular structure and junction design. The internal quantum efficiency (i.e., the ratio of photoelectrons to the number of photons absorbed in the molecular layer) can be calculated from the eC/Au window transmission shown in Figure S8 in the Supporting Information (30%) and the absorbance of the molecular layer at 407 nm (0.037)[15] to yield internal quantum efficiency = 14%.

An important mechanistic insight is the large offset of the OPV bias (where the PC = 0) from <5 mV for single-layer BTB to +0.37 V for BTB/AQ and −0.11 V for AQ/BTB. These offsets are too large to be due to an internal field from asymmetric electrode coupling, and imply an optically generated potential offset

due to the O/O interface. If electron transfer in a BTB/AQ MJ occurs between the BTB LUMO and the AQ LUMO to result in charge separation and exciton dissociation, it would polarize the top (AQ) electrode in the negative direction and result in a more positive OPV. Similarly, electron transfer from the BTB HOMO to a photogenerated hole in the AQ HOMO (i.e., h^+ transfer from AQ to BTB) would yield the same polarity shift. For either case, exchanging the layer order to AQ/BTB causes the OPV to change sign, and in both cases the photogenerated potential drop can exceed those in the dark MJ. The observation that the PC polarity correlates well with the HOMO energies but not the LUMO energies (Figure 8) is substantial evidence that transport is hole rather than electron mediated. Both possibilities are consistent with the observation than the thinnest MJs produce the largest PCs (Figure 5), which strongly indicates the importance of the O/O interface. The bilayer junctions are conceptually similar to organic heterojunctions in photocells and photodiodes,[17,22a,c] with the O/O interface providing the site for charge separation. However, the bilayer MJ has much shorter transport distances in the organic layers (<7 nm) and more efficient transport than that in thicker (i.e., >50 nm) devices. The observation that increasing layer thicknesses always reduces the PC yield (Figure 5) not only highlights the importance of the O/O interface but also implies that slow carrier transport through thicker films impedes efficient collection of the dissociated exciton.

4. Conclusions

For carbon-based MJs illuminated by UV-vis light the PC spectrum, magnitude, and sign depend strongly on molecular structure, and provides a clear example of a "molecular signature" relating electronic behavior to device structure. The PC spectrum closely tracks the absorption spectrum of the molecular layer, indicating that electron/hole generation is the primary step in producing a PC. Once the carriers are generated, they move in response to the built-in electric field present at zero bias, which results both from electronic coupling at the contacts and potential offsets at the O/O interface. The PC signs for 11 bilayer combinations are consistent with hole transport in the molecular layer, with electrons moving from higher to lower HOMO energy at the O/O interface. This correlation is valid both for bilayers containing donor and acceptor molecules as well as those containing two donors and two acceptors. An external bias applied during illumination greatly increases the PC by factors exceeding 10^5 relative to the dark current, depending on bias, structure, and illumination wavelength, resulting in a detection limit as low as 10.8 pW on a 0.00125 cm^2 MJ. Further investigations of effects of thickness, structure, and bias range are currently in progress for biased MJs, to examine the photon-induced conduction mechanism and the possibility of high-sensitivity, wavelength-selective molecular photodetectors.

5. Experimental Section

MJs were fabricated on diced, fused quartz chips (Quartz Unlimited LLC, nanograde polish). There are three main steps to produce the MJ sample shown in Figure 1B: i) deposition of bottom electrode, ii) electrochemical grafting of the molecular layer(s), and iii) deposition of top contact. For bottom electrode, Cr (4 nm), Au (30 nm), and eC (10 nm) were deposited using electron beam evaporation (Kurt J. Lesker PVD75) through a shadow mask following a previously established procedure.[11a] The molecular layers on the bottom electrode were deposited sequentially by electrochemical reduction of diazonium reagents, as described previously.[15,16] The grafting parameters are provided in Table S1 in the Supporting Information. The radical mediated grafting process resulted in covalent bonds within and between the molecular layers which was observable with Raman spectroscopy.[6c] After grafting the molecular layers, the top electrode was deposited as eC (10 nm) and Au (20 nm) by electron beam evaporation using a shadow mask.[11a] The optical transmission spectrum of the top contact is shown in Figure S8 in the Supporting Information, and a magnified optical image of the chip having nine MJs is shown in Figure S1 in the Supporting Information. Optical absorbance spectra of completed MJs were collected with an Agilent 8453 UV–vis spectrophotometer.

PC spectra were obtained using a 150 W Xenon arc source coupled with a monochromator (bandpass = 13 nm) through an optical beam chopper and focused onto the MJ through the top contact. A lock-in amplifier was employed for PC detection referenced to the optical beam chopper. The detailed procedure for measurements and verification of PC direction had been previously reported.[11b] Photon power density for each wavelength was measured using a Newport 1936-R power meter for calculating of the EQE, i.e., yield. PC under bias was measured by Keithley 2602A and Thorlabs 407 nm laser diode powered by a Thorlabs LDC 210C controller and TED 200C thermoelectric temperature controller. The laser power of beam at the sample was determined using a Newport 1936-R power-meter.[11a]

Supporting Information

Supporting Information is available from the Wiley Online Library or from the author.

Acknowledgements

This work was supported by the University of Alberta, Alberta Innovates, the National Research Council of Canada, and the Natural Sciences and Engineering Research Council. The authors thank Drs. Amin Morteza-Najarian and Colin Van Dyck for valuable scientific discussions and Bryan Szeto for assistance with LabView programming.

Conflict of Interest

The authors declare no conflict of interest.

Keywords

molecular electronics, molecular optoelectronics, photocurrent, photodetectors, photometric sensitivity

Received: June 24, 2019
Published online: August 7, 2019

[1] a) A. Vilan, D. Aswal, D. Cahen, *Chem. Rev.* **2017**, *117*, 4248; b) D. Xiang, X. Wang, C. Jia, T. Lee, X. Guo, *Chem. Rev.* **2016**, *116*, 4318.
[2] H. Yan, A. J. Bergren, R. McCreery, M. L. Della Rocca, P. Martin, P. Lafarge, J. C. Lacroix, *Proc. Natl. Acad. Sci. USA* **2013**, *110*, 5326.

[3] a) H. B. Akkerman, P. W. M. Blom, D. M. de Leeuw, B. de Boer, *Nature* **2006**, *441*, 69; b) H. Jeong, D. Kim, D. Xiang, T. Lee, *ACS Nano* **2017**, *11*, 6511.

[4] a) S. V. Aradhya, L. Venkataraman, *Nat. Nanotechnol.* **2013**, *8*, 399; b) X. Chen, M. Roemer, L. Yuan, W. Du, D. Thompson, E. del Barco, C. A. Nijhuis, *Nat. Nanotechnol.* **2017**, *12*, 797; c) R. McCreery, H. Yan, A. J. Bergren, *Phys. Chem. Chem. Phys.* **2013**, *15*, 1065; d) A. M. Najarian, B. Szeto, U. M. Tefashe, R. L. McCreery, *ACS Nano* **2016**, *10*, 8918.

[5] a) A. Scott, C. A. Hacker, D. B. Janes, *J. Phys. Chem. C* **2008**, *112*, 14021; b) Y. Jun, X. Zhu, *J. Am. Chem. Soc.* **2004**, *126*, 13224; c) M. Coll, L. H. Miller, L. J. Richter, D. R. Hines, O. D. Jurchescu, N. Gergel-Hackett, C. A. Richter, C. A. Hacker, *J. Am. Chem. Soc.* **2009**, *131*, 12451.

[6] a) N. Jiang, E. T. Foley, J. M. Klingsporn, M. D. Sonntag, N. A. Valley, J. A. Dieringer, T. Seideman, G. C. Schatz, M. C. Hersam, R. P. Van Duyne, *Nano Lett.* **2012**, *12*, 5061; b) Z. Liu, S.-Y. Ding, Z.-B. Chen, X. Wang, J.-H. Tian, J. R. Anema, X.-S. Zhou, D.-Y. Wu, B.-W. Mao, X. Xu, B. Ren, Z.-Q. Tian, *Nat. Commun.* **2011**, *2*, 305; c) M. Supur, S. R. Smith, R. L. McCreery, *Anal. Chem.* **2017**, *89*, 6463; d) A. J. Bergren, R. L. McCreery, *Annu. Rev. Anal. Chem.* **2011**, *4*, 173; e) A. M. Mahmoud, A. J. Bergren, R. L. McCreery, *Anal. Chem.* **2009**, *81*, 6972; f) A. M. Nowak, R. L. McCreery, *J. Am. Chem. Soc.* **2004**, *126*, 16621; g) A. M. Mahmoud, A. J. Bergren, N. Pekas, R. L. McCreery, *Adv. Funct. Mater.* **2011**, *21*, 2273.

[7] a) A. K. Farquhar, M. Supur, S. R. Smith, C. Van Dyck, R. L. McCreery, *Adv. Energy Mater.* **2018**, *8*, 1802439; b) A. P. Bonifas, R. L. McCreery, *Chem. Mater.* **2008**, *20*, 3849.

[8] a) M. Galperin, *Chem. Soc. Rev.* **2017**, *46*, 4000; b) M. Galperin, A. Nitzan, *Phys. Chem. Chem. Phys.* **2012**, *14*, 9421; c) O. Ivashenko, A. J. Bergren, R. L. McCreery, *J. Am. Chem. Soc.* **2016**, *138*, 722; d) W. Du, T. Wang, H.-S. Chu, L. Wu, R. Liu, S. Sun, W. K. Phua, L. Wang, N. Tomczak, C. A. Nijhuis, *Nat. Photonics* **2016**, *10*, 274; e) B. D. Fainberg, M. Jouravlev, A. Nitzan, *Phys. Rev. B* **2007**, *76*, 245329.

[9] a) P. Pourhossein, R. K. Vijayaraghavan, S. C. J. Meskers, R. C. Chiechi, *Nat. Commun.* **2016**, *7*, 11749; b) J. Zhou, K. Wang, B. Xu, Y. Dubi, *J. Am. Chem. Soc.* **2018**, *140*, 70; c) J. K. Viljas, F. Pauly, J. C. Cuevas, *Phys. Rev. B* **2008**, *77*, 155119; d) J. K. Viljas, F. Pauly, J. C. Cuevas, *Phys. Rev. B* **2007**, *76*, 033403; e) C. Jia, A. Migliore, N. Xin, S. Huang, J. Wang, Q. Yang, S. Wang, H. Chen, D. Wang, B. Feng, Z. Liu, G. Zhang, D.-H. Qu, H. Tian, M. A. Ratner, H. Q. Xu, A. Nitzan, X. Guo, *Science* **2016**, *352*, 1443; f) S. Ajisaka, B. Zunkovic, Y. Dubi, *Sci. Rep.* **2015**, *5*, 8312; g) Y. Gao, M. Galperin, *J. Chem. Phys.* **2016**, *144*, 244106/1.

[10] a) J. A. Fereiro, M. Kondratenko, A. J. Bergren, R. L. McCreery, *J. Am. Chem. Soc.* **2015**, *137*, 1296; b) J. A. Fereiro, R. L. McCreery, A. J. Bergren, *J. Am. Chem. Soc.* **2013**, *135*, 9584.

[11] a) A. M. Najarian, R. L. McCreery, *ACS Nano* **2019**, *13*, 867; b) A. Morteza Najarian, A. Bayat, R. L. McCreery, *J. Am. Chem. Soc.* **2018**, *140*, 1900.

[12] O. Ivashenko, A. J. Bergren, R. L. McCreery, *Adv. Electron. Mater.* **2016**, *2*, 1600351.

[13] a) W. Du, T. Wang, H.-S. Chu, C. A. Nijhuis, *Nat. Photonics* **2017**, *11*, 623; b) T. Wang, C. A. Nijhuis, *Appl. Mater. Today* **2016**, *3*, 73; c) Z. Dong, H.-S. Chu, D. Zhu, W. Du, Y. A. Akimov, W. P. Goh, T. Wang, K. E. J. Goh, C. Troadec, C. A. Nijhuis, J. K. W. Yang, *ACS Photonics* **2015**, *2*, 385; d) J.-C. Lacroix, Q. Van Nguyen, Y. Ai, Q. Van Nguyen, P. Martin, P.-C. Lacaze, *Polym. Int.* **2019**, *68*, 607; e) J.-C. Lacroix, P. Martin, P.-C. Lacaze, *Annu. Rev. Anal. Chem.* **2017**, *10*, 201.

[14] a) M. Galperin, A. Nitzan, *Phys. Rev. Lett.* **2005**, *95*, 206802; b) M. Galperin, A. Nitzan, M. A. Ratner, D. R. Stewart, *J. Phys. Chem. B* **2005**, *109*, 8519.

[15] S. R. Smith, R. L. McCreery, *Adv. Electron. Mater.* **2018**, *4*, 1800093.

[16] A. Bayat, J.-C. Lacroix, R. L. McCreery, *J. Am. Chem. Soc.* **2016**, *138*, 12287.

[17] K.-J. Baeg, M. Binda, D. Natali, M. Caironi, Y.-Y. Noh, *Adv. Mater.* **2013**, *25*, 4267.

[18] D. D. James, A. Bayat, S. R. Smith, J.-C. Lacroix, R. L. McCreery, *Nanoscale Horiz.* **2018**, *3*, 45.

[19] a) V. V. Afanasév, *Internal Photoemission Spectroscopy: Principles and Applications*, Elsevier Science, Oxford, UK **2008**; b) A. M. Goodman, *J. Appl. Phys.* **1970**, *41*, 2176.

[20] A. Morteza Najarian, R. L. McCreery, *ACS Nano* **2017**, *11*, 3542.

[21] a) Z. Xie, I. Bâldea, C. E. Smith, Y. Wu, C. D. Frisbie, *ACS Nano* **2015**, *9*, 8022; b) B. Kim, S. H. Choi, X. Y. Zhu, C. D. Frisbie, *J. Am. Chem. Soc.* **2011**, *133*, 19864; c) C. Tengstedt, W. Osikowicz, W. R. Salaneck, I. D. Parker, C.-H. Hsu, M. Fahlman, *Appl. Phys. Lett.* **2006**, *88*, 053502; d) C. Van Dyck, M. A. Ratner, *Nano Lett.* **2015**, *15*, 1577; e) C. Van Dyck, V. Geskin, J. Cornil, *Adv. Funct. Mater.* **2014**, *24*, 6154; f) D. Cahen, A. Kahn, E. Umbach, *Mater. Today* **2005**, *8*, 32; g) D. Cahen, A. Kahn, *Adv. Mater.* **2003**, *15*, 271; h) A. Salomon, T. Boecking, O. Seitz, T. Markus, F. Amy, C. Chan, W. Zhao, D. Cahen, A. Kahn, *Adv. Mater.* **2007**, *19*, 445.

[22] a) Y.-W. Su, S.-C. Lan, K.-H. Wei, *Mater. Today* **2012**, *15*, 554; b) D. H. Wang, D.-G. Choi, O. O. Park, J. H. Park, *J. Mater. Chem.* **2010**, *20*, 4910; c) J. Yu, Y. Zheng, J. Huang, *Polymers* **2014**, *6*, 2473; d) C.-A. Di, H. Shen, F. Zhang, D. Zhu, *Acc. Chem. Res.* **2019**, *52*, 1113; e) W. Wang, L. Qi, *Adv. Funct. Mater.* **2019**, *29*, 1807275.